

Article

Crystal Growth and Spectroscopic Investigations of $\text{Tm}^{3+}:\text{Li}_3\text{Ba}_2\text{Gd}_3(\text{MoO}_4)_8$ Crystal

Mingjun Song ^{1,*}, Lintong Wang ¹, Nana Zhang ¹, Xishi Tai ¹ and Guofu Wang ²

¹ School of Chemistry and Chemical Engineering, Weifang University, Weifang 261061, Shandong, China; E-Mails: wanglt6408@sina.com (L.W.); zhangnana0801@126.com (N.Z.); taixs@wfu.edu.cn (X.T.)

² Fujian Institute of Research on the Structure of Matter, The Chinese Academy of Sciences, Fuzhou 350002, Fujian, China; E-Mail: wgf@fjirsm.ac.cn

* Author to whom correspondence should be addressed; E-Mail: smj521@hotmail.com; Tel.: +86-536-8785-283; Fax: +86-536-8785-136.

Received: 3 October 2013; in revised form: 11 December 2013 / Accepted: 17 December 2013 / Published: 17 January 2014

Abstract: $\text{Tm}^{3+}:\text{Li}_3\text{Ba}_2\text{Gd}_3(\text{MoO}_4)_8$ crystal has been grown by the top seeded solution growth (TSSG) method from a Li_2MoO_4 flux. The room temperature polarized absorption spectra, fluorescence spectra, and fluorescence decay curves of the crystal were measured. Based on the Judd-Ofelt (J-O) theory, the main spectroscopic parameters of the crystal, including the spontaneous emission probabilities, fluorescence branching ratios, and radiative lifetimes were calculated and analyzed. The broad and strong absorption bands of the crystal show that it can be efficiently pumped by the diode laser, while the large emission cross-sections of the $^3\text{F}_4 \rightarrow ^3\text{H}_6$ transition indicate that the crystal is a promising candidate for tunable and short pulse lasers.

Keywords: crystal growth; optical materials; spectral properties; cross section

1. Introduction

With the rapid progress of high power diode lasers, Tm^{3+} -doped laser media has been intensively investigated because of their potential applications associated with emissions in the visible and infrared spectral regions, particularly at ~ 1.50 and ~ 2.0 μm wavelength. As we know, the $^3\text{F}_4 \rightarrow ^3\text{H}_6$ transition of Tm^{3+} ions is one of the most effective channels for the development of 2.0 μm lasers, which have

many important applications in fields of medicine, gas detection, remote sensing, *etc.* On the other hand, the ${}^3\text{H}_4 \rightarrow {}^3\text{F}_4$ transition of Tm^{3+} ions gives rise to an additional infrared emission band around 1.5 μm , where applications such as detection, ranging and optical communication have been found. Other important advantages of Tm^{3+} ions include strong absorption of AlGaAs diode laser radiation at ~ 800 nm, a long lifetime of the ${}^3\text{F}_4$ state, a high quantum efficiency due to the cross-relaxation between ${}^3\text{H}_4$ and ${}^3\text{F}_4$ multiplets, as well as a wide emission band around in the range of 1800–2000 nm, which is definitely promising for the generation of tunable and ultrafast solid state lasers. To date, efficient laser operations around 2.0 μm have been realized in a number of Tm^{3+} -doped crystals [1–10].

Among the reported crystals, the double tungstate and molybdate crystals with scheelite structure are characterized by their local disordered crystal structure [4–8]. The advantages of these crystals are high quantum efficiency, broad absorption and emission bands, as well as relatively low upper-level lifetime. Furthermore, such a combination of these merits is very promising for generations of tunable and ultra fast lasers. More recently, a new series of disordered molybdate compounds $\text{Li}_3\text{Ba}_2\text{Re}_3(\text{MoO}_4)_8$ (Re = La-Lu, Y), which belong to the monoclinic system, with the space group C2/c, have emerged as new kinds of laser materials, especially in tunable and ultrafast laser domains [11–17]. The structure of $\text{Li}_3\text{Ba}_2\text{Re}_3(\text{MoO}_4)_8$ can also be considered to be derived from the scheelite structure, in which the Ca^{2+} sites are occupied by a statistical mixture of 25% Ba^{2+} , 37.5% Li^+ , and 37.5% Re^{3+} [13]. Consequently, rare earth doped $\text{Li}_3\text{Ba}_2\text{Re}_3(\text{MoO}_4)_8$ crystals usually exhibit very similar spectral properties to the typical disordered double molybdate crystals. Up to now, efficient laser operation has already been realized in Nd^{3+} and Yb^{3+} -doped $\text{Li}_3\text{Ba}_2\text{Gd}_3(\text{MoO}_4)_8$ crystals [11,13]. Not long ago, Zaldo *et al.* [16] have demonstrated the great potential of $\text{Tm}^{3+}:\text{Li}_3\text{Ba}_2\text{Lu}_3(\text{MoO}_4)_8$ crystal for tunable and ultrashort pulse lasers around 2 μm , *i.e.*, a tunable laser in the range of 1853–2009 nm, with a slope efficiency up to 71%, higher than those obtained in disordered crystals so far, has been obtained with a Ti:laser as pump source. Furthermore, the large free running laser bandwidth indicated that the $\text{Tm}^{3+}:\text{Li}_3\text{Ba}_2\text{Lu}_3(\text{MoO}_4)_8$ crystal is definitely promising for generations of ultrafast laser pulses. In the present work, the studies are extended to Tm^{3+} -doped $\text{Li}_3\text{Ba}_2\text{Gd}_3(\text{MoO}_4)_8$ crystal with the objective of exploring new Tm^{3+} -doped crystal for efficient laser operations near 2 μm , and the growth and spectral properties of $\text{Tm}^{3+}:\text{Li}_3\text{Ba}_2\text{Gd}_3(\text{MoO}_4)_8$ crystal are reported.

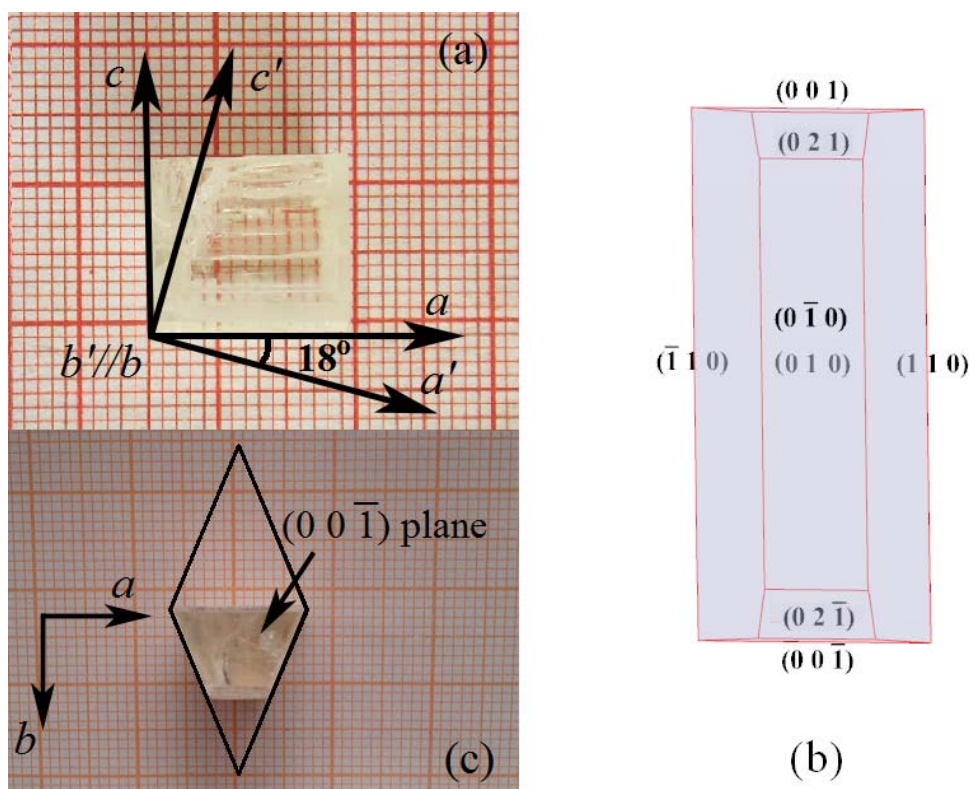
2. Experimental Section

2.1. Crystal Growth and Orientation

As $\text{Li}_3\text{Ba}_2\text{Gd}_3(\text{MoO}_4)_8$ crystal melts incongruently [12], the crystal was grown by the top seeded solution growth (TSSG) method from a flux of Li_2MoO_4 . The solubility curve of $\text{Li}_3\text{Ba}_2\text{Gd}_3(\text{MoO}_4)_8$ crystal in the $\text{Li}_3\text{Ba}_2\text{Gd}_3(\text{MoO}_4)_8$ - Li_2MoO_4 solution can be found in Reference [14]. The crystal growth was carried out in a vertical tubular muffle furnace with a nickel–chrome wire as the heating element. An AL-708 apparatus controlled the furnace temperature and the rate of cooling. The starting materials, 3 at% Tm^{3+} -doped $\text{Li}_3\text{Ba}_2\text{Gd}_3(\text{MoO}_4)_8$ and Li_2MoO_4 were weighed, with a molar ratio of $\text{TmLi}_3\text{Ba}_2\text{Gd}_3(\text{MoO}_4)_8:\text{Li}_2\text{MoO}_4 = 1:4$. A single-crystalline bar cut along *b*-direction was used to introduce crystal nucleation. The growth temperature interval was 900–870 $^\circ\text{C}$, with a cooling rate of 1 $^\circ\text{C}/\text{d}$ and a rotating rate of 12 rpm. Additional details on crystal growth can be found

in Reference [14,15]. The as-grown $\text{Tm}^{3+}:\text{Li}_3\text{Ba}_2\text{Gd}_3(\text{MoO}_4)_8$ crystal with a prism shape is shown in Figure 1a. The initial dimension of the grown crystal is about $15 \times 10 \times 40 \text{ mm}^3$ along the a , b , and c -directions, respectively. However, due to the cleavable nature of the crystal, the grown crystal has split along the middle along the cleavage plane (001) during the annealing process. As a result, only a small part of the obtained crystal is shown in Figure 1a. Figure 1b shows the morphological scheme of the grown crystal. The rectangular facets on the top and bottom of the crystal were established to be (010) and (0 $\bar{1}$ 0) faces, respectively, which are consistent with those of the $\text{Li}_3\text{Ba}_2\text{Lu}_3(\text{MoO}_4)_8$ crystal [17]. However, different from the $\text{Li}_3\text{Ba}_2\text{Lu}_3(\text{MoO}_4)_8$ crystal, the facets along sides of the crystal were identified to be (110) and ($\bar{1}$ 10) faces, respectively, rather than (100) and ($\bar{1}$ 00) faces. As a consequence, the grown crystal possesses a trapezoid cross-section, as shown in Figure 1c. It can be found that the profile of the (00 $\bar{1}$) face of the $\text{Tm}^{3+}:\text{Li}_3\text{Ba}_2\text{Gd}_3(\text{MoO}_4)_8$ crystal is in good accordance with that of the $\text{Yb}^{3+}:\text{Li}_3\text{Ba}_2\text{Gd}_3(\text{MoO}_4)_8$ and $\text{Er}^{3+}:\text{Li}_3\text{Ba}_2\text{Y}_3(\text{MoO}_4)_8$ crystal grown along the a -direction [12,15].

Figure 1. (a) Grown crystal of $\text{Tm}^{3+}:\text{Li}_3\text{Ba}_2\text{Gd}_3(\text{MoO}_4)_8$; (b) The morphological scheme of the crystal; (c) Cross-section of the as grown crystal.



As the $\text{Li}_3\text{Ba}_2\text{Gd}_3(\text{MoO}_4)_8$ crystal is biaxial, the three principal axes of the optical indicatrix should be determined before the polarized spectral measurement. In the monoclinic system, one of the principal axes is collinear with the crystallographic b -axis and the other two principal axes are perpendicular and positioned at certain angles with respect to crystallographic a and c -axes. Then, the other two principal axes can be easily determined when the sample is viewed along the b -axis direction under a polarized microscope. However, due to the restriction of the test conditions, the precise values of the refractive index for the three principal axes were not measured. As the cell parameters and the

positions of the three principal axes relative to the crystallographic axes are very close to the $\text{Li}_3\text{Ba}_2\text{Lu}_3(\text{MoO}_4)_8$ crystal, the three principal axes are temporarily named in the same way as the $\text{Li}_3\text{Ba}_2\text{Lu}_3(\text{MoO}_4)_8$ crystal [16,17]. As shown in Figure 1a, the principal axis collinear with the crystallographic b axis is named as b' ; a' is rotated at 18° with respect to a axis in the clockwise direction as the crystals are viewed from the negative b axis, finally, c' is perpendicular to a' and b' .

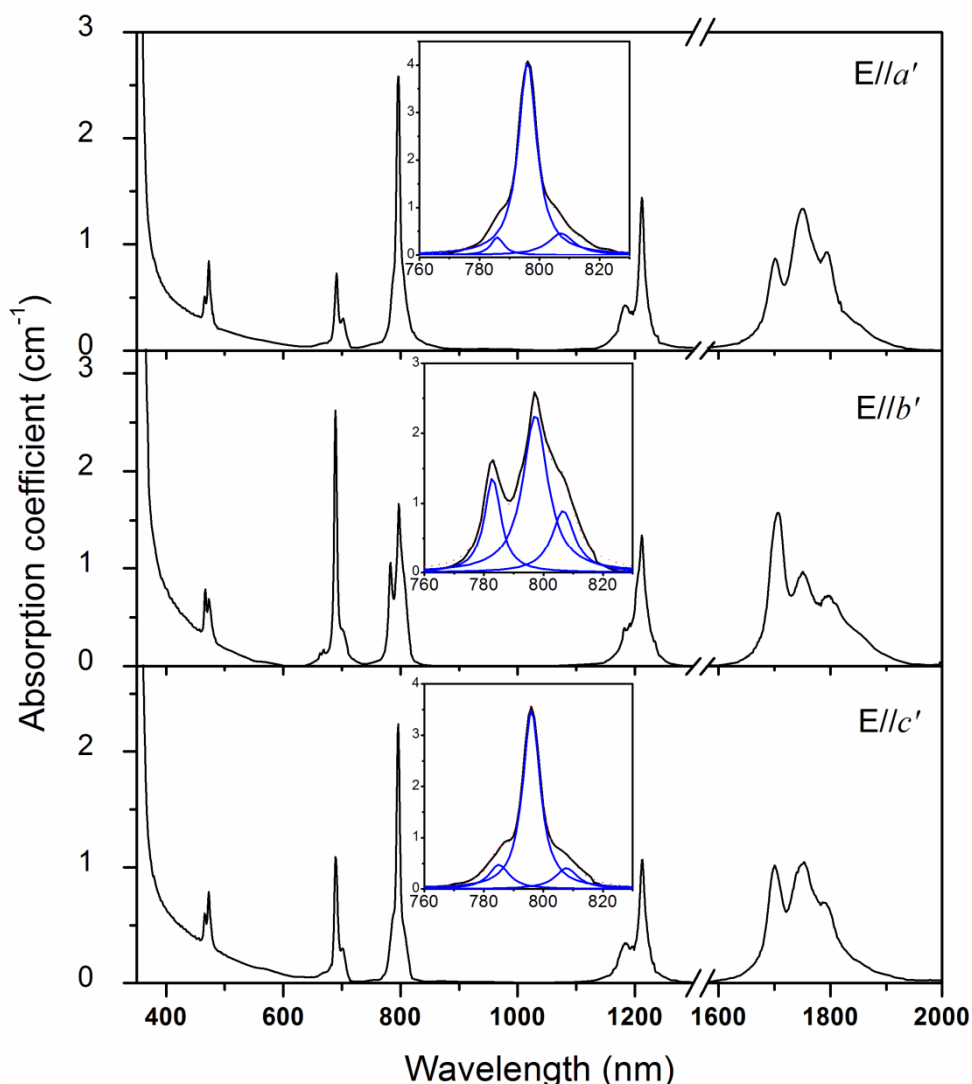
2.2. Characterizations

The polarized absorption spectra were measured using a Perkin–Elmer UV-VIS-NIR spectrometer (Lambda-900) in a wavelength range of 300–2000 nm, the wavelength resolution of which is 0.08 nm. The polarized fluorescence spectra and the fluorescence decay curves were measured using an Edinburgh Instruments FLS920 spectrophotometer, the wavelength resolution of which is 0.2 nm. The concentration of Tm^{3+} ions in the $\text{Tm}^{3+}:\text{Li}_3\text{Ba}_2\text{Gd}_3(\text{MoO}_4)_8$ was measured to be 1.26 at% by the ICP atomic emission spectroscopy analysis method. Thus, the corresponding concentration and the segregation coefficient of Tm^{3+} ions in the grown crystal were $6.3 \times 10^{-19} \text{ cm}^2$ and 0.42, respectively. All the above measurements were carried out at room temperature.

3. Results and Discussion

3.1. Absorption Spectra and Judd-Ofelt Analysis

Figure 2 shows the polarized absorption spectra of $\text{Tm}^{3+}:\text{Li}_3\text{Ba}_2\text{Gd}_3(\text{MoO}_4)_8$ crystal measured at room temperature. For all polarizations, strong absorption bands occur around 475, 690, 800, 1200, and 1750 nm, corresponding to the transitions of Tm^{3+} ions from the ground state $^3\text{H}_6$ to the excited states $^1\text{G}_4$, $^3\text{F}_{2,3}$, $^3\text{H}_4$, $^3\text{H}_5$, and $^3\text{F}_4$, respectively. The most attractive band of the absorption spectra is the one around 800 nm, which belongs to the $^3\text{H}_6 \rightarrow ^3\text{H}_4$ transition and is the main pumping channel for Tm^{3+} ions. The inset of Figure 2 shows the absorption cross-sections σ_{abs} of this band for clarity. As this band is composed of several overlapped peaks, a Lorentz fit was applied to it and three peaks, around 785, 796, and 805 nm, were found. For all polarizations, the peak absorption cross-sections are located at 796 nm and the values are 4.08, 2.59, and $3.55 \times 10^{-20} \text{ cm}^2$ for $E//a'$, $E//b'$, and $E//c'$, respectively. The full width at half the maximum (FWHM) of the 796 nm absorption peaks are 9, 11, and 8 nm for $E//a'$, $E//b'$, and $E//c'$, respectively, which are close to those of other disordered molybdate crystals, such as $\text{Tm}^{3+}:\text{LiLa}(\text{MoO}_4)_2$ (8 nm for σ polarization) [6], $\text{Tm}^{3+}:\text{LiGd}(\text{MoO}_4)_2$ (8 nm for σ polarization) [8], and $\text{Tm}^{3+}:\text{Ba}_2\text{Gd}_4(\text{MoO}_4)_4$ (7 nm for $E//X$ and 8 nm for $E//Y$) [7], but much larger than those of ordered $\text{Tm}^{3+}:\text{YAG}$ (4 nm) [1], $\text{Tm}^{3+}:\text{YVO}_4$ (5 nm for π polarization) [2], and $\text{Tm}^{3+}:\text{KY}(\text{WO}_4)_2$ (5.4 nm for $E//N_m$) crystals [3]. Such a broad bandwidth indicates an inhomogeneous broadening behavior of $\text{Tm}^{3+}:\text{Li}_3\text{Ba}_2\text{Gd}_3(\text{MoO}_4)_8$ crystal and make the crystal very suitable for diode pumping, as the thermal stabilization of pumping source is not so critical in this case. Furthermore, it can be found that both the profile and the intensity of the absorption bands of $\text{Tm}^{3+}:\text{Li}_3\text{Ba}_2\text{Gd}_3(\text{MoO}_4)_8$ are similar to those of the isostructural $\text{Tm}^{3+}:\text{Li}_3\text{Ba}_2\text{Lu}_3(\text{MoO}_4)_8$ crystal [16].

Figure 2. Polarized absorption spectra of $\text{Tm}^{3+}:\text{Li}_3\text{Ba}_2\text{Gd}_3(\text{MoO}_4)_8$ crystal.

The Judd-Ofelt (J-O) theory has been widely used in the analysis of the spectroscopic properties of rare-earth ions in crystals and glasses [18,19]. According to the J-O theory, the Judd-Ofelt parameters Ω_t ($t = 2, 4, 6$) for each polarization can be calculated by a least-square fitting between the theoretical and the experimental line strengths for the electric-dipole transitions. Then, the spontaneous emission probabilities of the electric-dipole A^{ed} and magnetic-dipole A^{md} transitions, the fluorescence branching ratios β and the radiative lifetime τ_r can be estimated. In the present work, only the calculated results are presented, and the detailed calculation procedures are similar to those reported in Reference [4]. The values of the refractive index, n , at different wavelengths were calculated using the Sellmeier Equations:

$$n^2 = A + \frac{B\lambda^2}{\lambda^2 - C^2} - D\lambda^2 \quad (1)$$

where the constants A , B , C , and D for the three polarizations were derived from Reference [17].

The values of A^{ed} , A^{md} , β , and τ_r of some typical transitions are listed in Table 1.

Table 1. The spontaneous emission probabilities, fluorescence branching ratios and radiative lifetimes of $\text{Tm}^{3+}:\text{Li}_3\text{Ba}_2\text{Gd}_3(\text{MoO}_4)_8$ crystal.

Transitions	λ_{em} (nm)	$E//a'$	$E//b'$	$E//c'$	β	τ_r (μs)
		$A_{\text{ed}} + A_{\text{md}}$ (s^{-1})	$A_{\text{ed}} + A_{\text{md}}$ (s^{-1})	$A_{\text{ed}} + A_{\text{md}}$ (s^{-1})		
$^1\text{G}_4 \rightarrow ^3\text{H}_6$	477	5035.7	5474.1	4258.7	0.56	113
$^3\text{F}_4$	649	345.8 + 13.8	580.8 + 13.9	388.7 + 12.8	0.05	
$^3\text{H}_5$	780	2031.8 + 207.2	2334.7 + 208.7	1936.4 + 192.4	0.26	
$^3\text{H}_4$	1170	993.1 + 47.3	925.3 + 47.7	839.2 + 44.03	0.11	
$^3\text{F}_3$	1485	93.2 + 3.8	173.7 + 3.9	113.2 + 3.6	0.02	
$^3\text{F}_2$	1635	27.9	59.8	33.4	0.004	
$^3\text{H}_4 \rightarrow ^3\text{H}_6$	785	5544.6	5597.5	4792.5	0.90	170
$^3\text{F}_4$	1430	469.8 + 26.8	497.8 + 27.1	407.2 + 25	0.08	
$^3\text{H}_5$	2165	47.9 + 14	131.5 + 14.2	62.8 + 13	0.02	
$^3\text{H}_5 \rightarrow ^3\text{H}_6$	1225	676.0 + 117	969.5 + 118	671.6 + 108.9	0.99	1110
$^3\text{F}_4$	3825	12.8 + 0.16	15.2 + 0.16	10.9 + 0.14	0.01	
$^3\text{F}_4 \rightarrow ^3\text{H}_6$	1800	970.0	1040.0	791	1.00	1070

3.2. Fluorescence Spectra and Emission Cross-Sections

Figure 3 shows the polarized emission spectra of $\text{Tm}^{3+}:\text{Li}_3\text{Ba}_2\text{Gd}_3(\text{MoO}_4)_8$ crystal in a range of 600–1600 nm, when the samples were excited into the $^1\text{G}_4$ state with 475 nm radiation. There are four main emission bands around 650, 800, 1175, and 1450 nm for each polarization. The emission bands around 650, 1175, and 1450 nm can be assigned to the $^1\text{G}_4 \rightarrow ^3\text{F}_4$, $^1\text{G}_4 \rightarrow ^3\text{H}_4$, and $^3\text{H}_4 \rightarrow ^3\text{F}_4$ transitions, respectively. The emission band around 800 nm should be the superposition of two resonant transitions, namely $^1\text{G}_4 \rightarrow ^3\text{H}_5$ and $^3\text{H}_4 \rightarrow ^3\text{H}_6$, which were severely overlapped due to the very close barycentric wavelengths. To confirm the conclusion, the polarized emission spectra were also measured under 688 nm excitation, *i.e.*, the Tm^{3+} ions were excited to the $^3\text{F}_{2,3}$ states. In this case, the $^3\text{H}_4$ state was populated through non-radiative relaxation from the $^3\text{F}_{2,3}$ states and later on depopulated directly to the $^3\text{H}_6$ ground state, giving rise the emissions at 800 nm as shown in Figure 3b. Then, it can be concluded that the weaker emission at 785 nm in Figure 3a belongs to the $^1\text{G}_4 \rightarrow ^3\text{H}_5$ transition.

The stimulated emission cross-sections of the $^3\text{H}_4 \rightarrow ^3\text{F}_4$ transition around 1.5 μm were calculated from the fluorescence spectra using the Füchtbauer-Ladenburg(F-L) formula [2]:

$$\sigma_{\text{em},q}(\lambda) = \frac{\lambda^5 A_q(J \rightarrow J') I_q(\lambda)}{8\pi c n^2 \int \lambda I_q(\lambda) d(\lambda)} \quad (2)$$

where c is the speed of light in the vacuum; $I_q(\lambda)$ is the relative fluorescence intensity at wavelength λ . Then, the emission cross-sections for three polarizations are shown in Figure 4. For $E//b'$, the peak emission cross-sections are $1.25 \times 10^{-20} \text{ cm}^2$ at 1452 nm. For $E//a'$ and $E//c'$, the peak emission cross-sections are located at 1495 nm and the values are $9.16 \times 10^{-21} \text{ cm}^2$ and $1.12 \times 10^{-20} \text{ cm}^2$, respectively. The $^3\text{H}_4 \rightarrow ^3\text{F}_4$ transition of the Tm^{3+} ions has provided a promising approach to achieve 1.5 μm lasers in a more efficient four-level laser operation scheme than the Er^{3+} ions. However, their practical applications at this wavelength are inevitably restricted by a detrimental bottlenecking effect

because the lifetime of the 3F_4 state is generally much longer than that of the 3H_4 state. As a result, to achieve laser operation via $^3H_4 \rightarrow ^3F_4$ transition, some codopants, such as Ho^{3+} , Yb^{3+} , and Tb^{3+} should be introduced as deactivator to depopulate the 3F_4 state [20].

Figure 3. Polarized fluorescence spectra of $Tm^{3+}:Li_3Ba_2Gd_3(MoO_4)_8$ crystal: (a) Excited with 473 radiation; (b) Excited with 688 nm radiation.

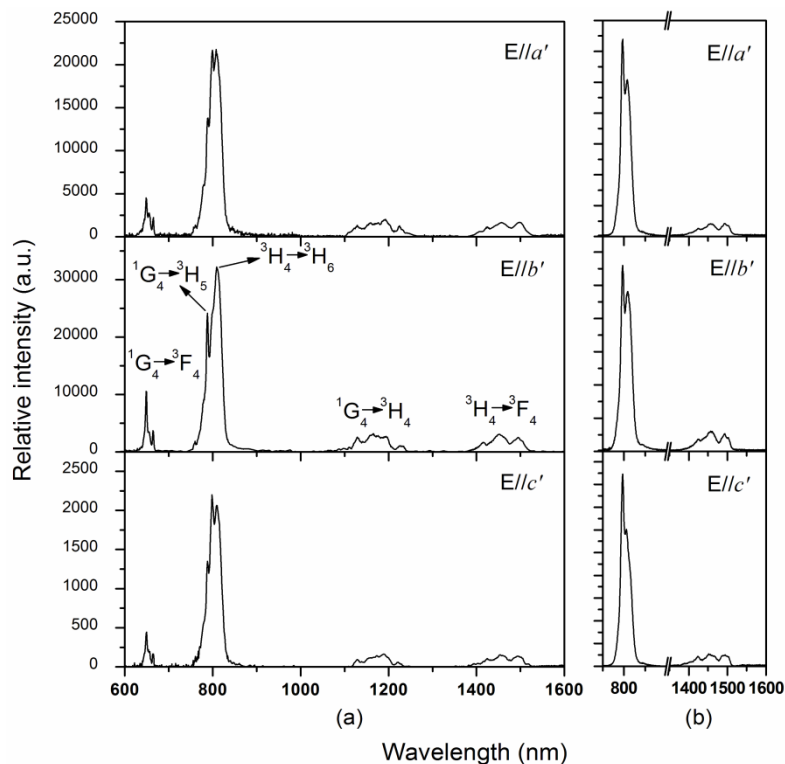
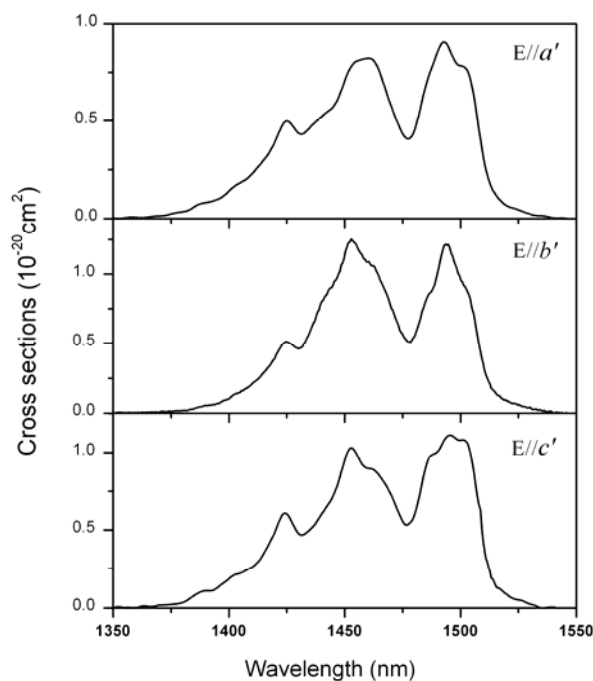


Figure 4. Polarized emission cross-sections of $Tm^{3+}:Li_3Ba_2Gd_3(MoO_4)_8$ crystal for the $^3H_4 \rightarrow ^3F_4$ transition around 1.5 μm .



Due to the restriction of the test conditions, only the uncalibrated emission spectra of the ${}^3F_4 \rightarrow {}^3H_6$ transition, around 2 μm , were obtained, as shown in Figure 5. Thus, the emission cross-sections of this transition were calculated from the absorption spectra according to the reciprocity method [21]:

$$\sigma_{\text{em}}(\lambda) = \sigma_{\text{abs}}(\lambda) \frac{Z_l}{Z_u} \exp[(E_{z_l} - hc/\lambda)/kT] \quad (3)$$

where k is the Boltzmann's constant; Z_l and Z_u are the partition functions of lower and upper states, respectively; E_{z_l} is the zero-line energy defined as the energy separation between the lowest Stark levels of the upper and lower multiplets. However, the precise energy level diagram of Tm^{3+} ions in $\text{Li}_3\text{Ba}_2\text{Gd}_3(\text{MoO}_4)_8$ crystal is not available now. Therefore the values of Z_l/Z_u and E_{z_l} were roughly taken as $Z_l/Z_u = 1.42$ and $E_{z_l} = 5600 \text{ cm}^{-1}$ (0.694 eV), respectively, in agreement with those of the isostructural $\text{Tm}^{3+}:\text{Li}_3\text{Ba}_2\text{Lu}_3(\text{MoO}_4)_8$ crystal [16]. Then, the emission cross-sections are obtained and listed in Figure 5 combining with the corresponding absorption cross-sections. For all polarizations, the peak emission cross-sections are located at 1796 nm and the values are 2.38, 2.27, and $2.05 \times 10^{-20} \text{ cm}^2$ for $E//a'$, $E//b'$, and $E//c'$, respectively, which are larger than those of other disordered molybdate crystals (see Table 2). Furthermore, the FWHMs of the emission cross-sections are 133, 154 and 136 nm for $E//a'$, $E//b'$, and $E//c'$, respectively, which are similar to those of other disordered molybdate crystals in Table 2.

Figure 5. Polarized absorption (dot line), emission (solid line) cross-sections and emission spectra (red line) of $\text{Tm}^{3+}:\text{Li}_3\text{Ba}_2\text{Gd}_3(\text{MoO}_4)_8$ crystal for the ${}^3F_4 \rightarrow {}^3H_6$ transition.

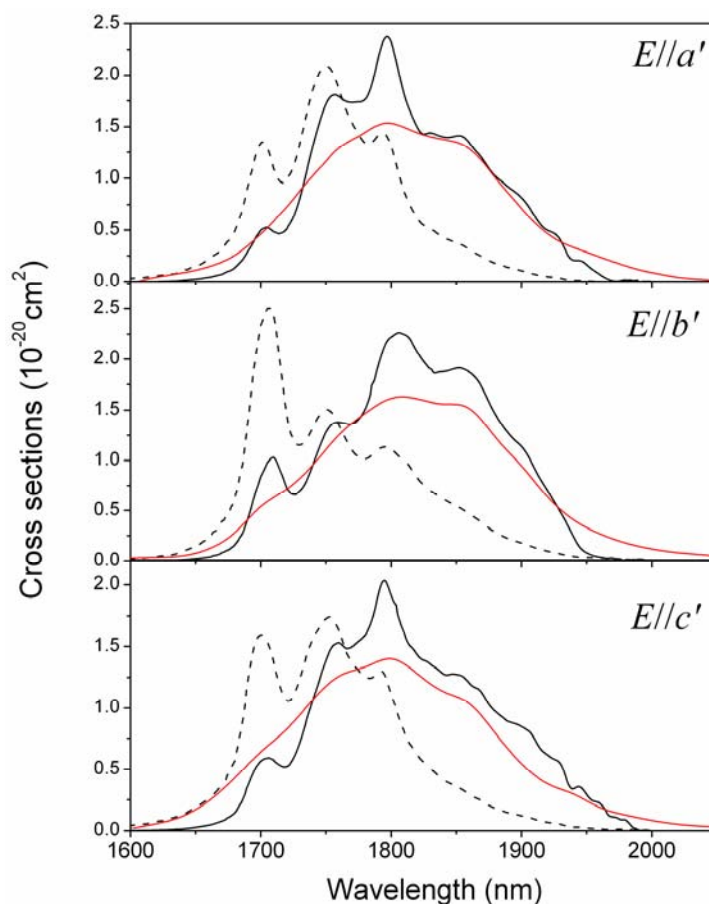


Table 2. The main spectral parameters of $\text{Tm}^{3+}:\text{Li}_3\text{Ba}_2\text{Gd}_3(\text{MoO}_4)_8$ and other Tm^{3+} -doped crystals.

Properties	$\text{Li}_3\text{Ba}_2\text{Gd}_3(\text{MoO}_4)_8$	$\text{LiGd}(\text{MoO}_4)_2$	$\text{LiLa}(\text{MoO}_4)_2$	$\text{BaGd}_2(\text{MoO}_4)_4$	$\text{Li}_3\text{Ba}_2\text{Lu}_3(\text{MoO}_4)_8$
λ_{abs} (nm)	796	795 (σ)	795	798	797 (a')
	–	796 (π)	–	–	782 (b')
	–	–	–	–	804 (c')
σ_a (10^{-20} cm ²)	4.08 (a')	4.33 (σ)	4.04 (σ)	2.5 (X)	3.8 (a')
	2.59 (b')	1.59 (π)	1.53 (π)	3.5 (Y)	2.7 (b')
	3.55 (c')	–	–	2.1 (Z)	3.1 (c')
FWHM (nm)	9 (a')	8 (σ)	8 (σ)	7 (X)	8 (a')
	11 (b')	37 (π)	36 (π)	8 (Y)	12 (b')
	8 (c')	–	–	17 (Z)	8 (c')
λ_e (nm)	–	1786 (σ)	1787 (σ)	1800 (X)	1800 (a')
	1796	1838 (π)	1837 (π)	1805 (Y)	1812 (b')
	–	–	–	1819 (Z)	1805 (c')
σ_{em} (10^{-20} cm ²)	2.38 (a')	2.44 (σ)	1.48 (σ)	1.3 (X)	2.65 (a')
	2.27 (b')	2.07 (π)	1.61 (π)	1.8 (Y)	2.30 (b')
	2.05 (c')	–	–	1.3 (Z)	2.25 (c')
FWHM (nm)	133 (a')	175 (σ)	143 (σ)	110 (X)	90 (a')
	154 (b')	160 (π)	164 (π)	84 (Y)	168 (b')
	136 (c')	–	–	200 (Z)	137 (c')
τ_f of $^3\text{F}_4$ (ms)	0.92	0.93	1.29	–	0.97
References	This work	[8]	[6]	[7]	[16]

From the absorption and emission cross-sections calculated by the reciprocity method, the gain cross-section, σ_g , can be calculated according to the following equation:

$$\sigma_g = \beta\sigma_{\text{em}} - (1 - \beta)\sigma_{\text{abs}} \quad (4)$$

where β is the ratio of the number of the excited Tm^{3+} ions to the total number of Tm^{3+} ions; σ_{em} and σ_{abs} are the emission and absorption cross-sections, respectively. The calculated gain cross-sections for several values of β are shown in Figure 6. According to Figure 6, a minimum inversion ratio of 0.1 is needed to achieve laser operations. For an inversion ratio of $\beta = 0.3$, a tunable range wider than 180 nm is possible for all polarizations.

The fluorescence decay curve of the $^3\text{H}_4$ and $^3\text{F}_4$ state was recorded by monitoring the emissions of the $^3\text{H}_4 \rightarrow ^3\text{F}_4$ and $^3\text{F}_4 \rightarrow ^3\text{H}_6$ transitions at 1500 and 1900 nm under excitation at 800 and 1730 nm, respectively. The decay curve of the $^3\text{H}_4$ state exhibits a single exponential behavior as shown in Figure 7. The lifetime is obtained to be 153 μs by linear fitting, which is close to the radiative one. The high quantum efficiency η (τ_f/τ_r) of the $^3\text{H}_4$ state means the cross-relaxation is inefficient in the crystal due to the low Tm^{3+} concentration. The lifetime of $^3\text{F}_4$ state for the bulk crystal is measured to be 1.62 ms and much larger than the calculated radiative lifetime. Such a large discrepancy is mainly caused by the re-absorption effect, which has been widely observed in Tm^{3+} -doped crystals [8,16]. To obtain the intrinsic lifetime of the $^3\text{F}_4$ state, the powder method was adopted in this work [22]. A piece of bulk crystal was grounded into fine particles and diluted to a lower concentration of 0.25 at% (1.25×10^{-19} cm²) with the powder of pure $\text{Li}_3\text{Ba}_2\text{Gd}_3(\text{MoO}_4)_8$ crystal. Then, the powder was immersed into ethylene glycol (EG), which was used as refractive index matching fluid to reduce the

internal reflection within the particles. The fluorescence lifetime of the powder sample was measured to be 0.92 ms, in reasonable agreement with the radiative one calculated by the J-O theory.

Figure 6. Gain cross-sections of $\text{Tm}^{3+}:\text{Li}_3\text{Ba}_2\text{Gd}_3(\text{MoO}_4)_8$ crystal for different values of inversion ratio β ($\beta = 0.1, 0.2, 0.3, 0.4, 0.5$).

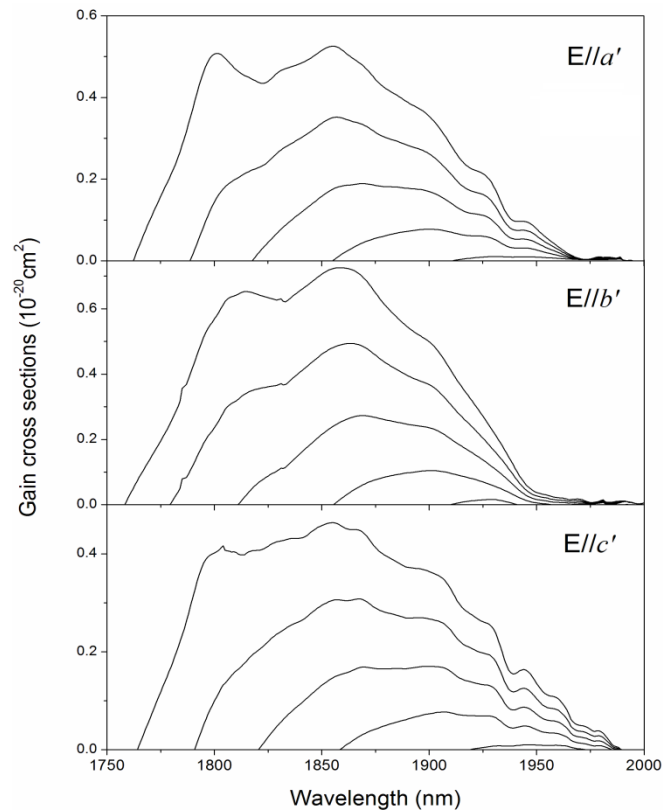
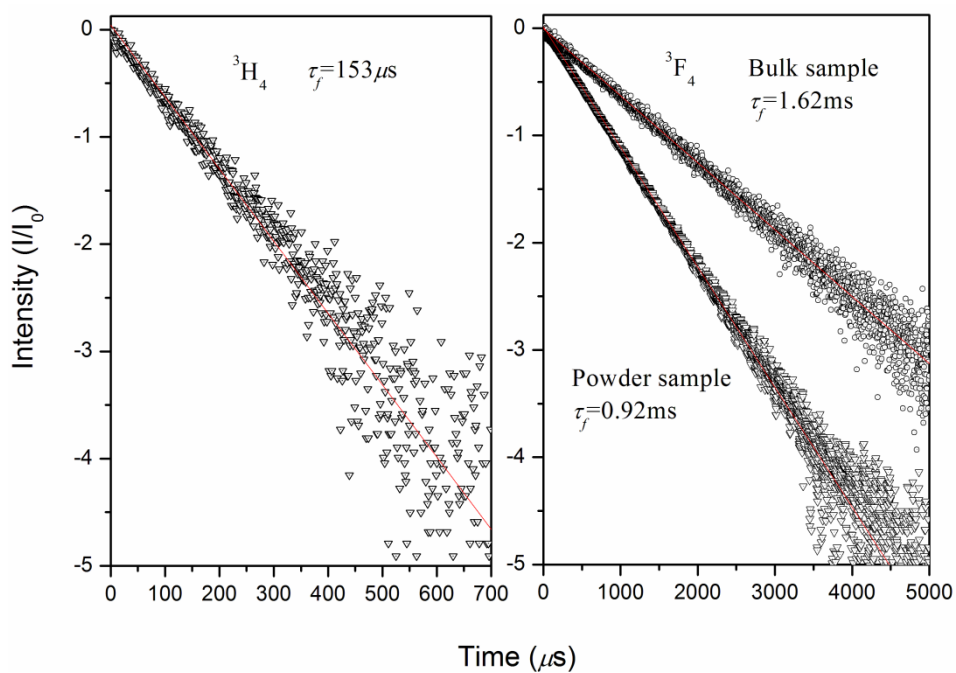


Figure 7. Fluorescence decay curves of $^3\text{H}_4$ and $^3\text{F}_4$ state.



4. Conclusions

A $\text{Tm}^{3+}:\text{Li}_3\text{Ba}_2\text{Gd}_3(\text{MoO}_4)_8$ crystal has been successfully grown by the top seeded solution growth (TSSG) method, and the detailed spectral properties of the crystal were characterized and investigated on the basis of the J-O theory. The main spectral parameters of the crystal are listed in Table 2 and compared with other Tm^{3+} -doped crystals. It can be found that $\text{Tm}^{3+}:\text{Li}_3\text{Ba}_2\text{Gd}_3(\text{MoO}_4)_8$ crystal possesses similar spectral characters to other disordered molybdate crystals, *i.e.*, all of them exhibited broad optical bands, large absorption and emission cross-sections, as well as long lifetimes of $^3\text{F}_4$ state. In summary, the main spectroscopic parameters of the $\text{Tm}^{3+}:\text{Li}_3\text{Ba}_2\text{Gd}_3(\text{MoO}_4)_8$ crystal are comparable to those of the $\text{Tm}^{3+}:\text{Li}_3\text{Ba}_2\text{Lu}_3(\text{MoO}_4)_8$ crystal. As a consequence, in view of the excellent laser performance of the $\text{Tm}^{3+}:\text{Li}_3\text{Ba}_2\text{Lu}_3(\text{MoO}_4)_8$ crystal [16], we may expect the $\text{Tm}^{3+}:\text{Li}_3\text{Ba}_2\text{Gd}_3(\text{MoO}_4)_8$ crystal to be a potential solid state laser material at $\sim 2.0 \mu\text{m}$.

Acknowledgments

This work was supported by the Natural Science Foundation of Shandong Province (ZR2010BL011) and the Science Foundation of Weifang University.

Conflicts of Interest

The authors declare no conflict of interest.

References

1. Fan, T.Y.; Huber, G.; Byer, R.L.; Mitzscherlich, P. Spectroscopy and diode laser-pumped operation of $\text{Tm},\text{Ho}:\text{YAG}$. *IEEE J. Quantum Electron.* **1988**, *24*, 924–933.
2. Ohta, K.; Saito, H.; Obara, M. Spectroscopic characterization of $\text{Tm}^{3+}:\text{YVO}_4$ crystal as an efficient diode pumped laser source near 2000 nm. *J. Appl. Phys.* **1993**, *73*, 3149–3153.
3. Troshin, A.E.; Kisel, V.E.; Yasukevich, A.S.; Kuleshov, N.V.; Pavlyuk, A.A.; Dunina, E.B.; Kornienko, A.A. Spectroscopy and laser properties of $\text{Tm}^{3+}:\text{KY}(\text{WO}_4)_2$ crystal. *Appl. Phys. B* **2007**, *86*, 287–292.
4. Guo, W.J.; Chen, Y.J.; Lin, Y.F.; Luo, Z.D.; Gong, X.H.; Huang, Y.D. Spectroscopic properties and laser performance of Tm^{3+} -doped $\text{NaLa}(\text{MoO}_4)_2$ crystal. *J. Appl. Phys.* **2008**, *103*, 093106:1–093106:10.
5. Han, X.M.; Cano-Torres, J.M.; Rico, M.; Cascales, C.; Zaldo, C.; Mateos, X.; Rivier, S.; Griebner, U.; Petrov, V. Spectroscopy and efficient laser operation near 1.95 μm of Tm^{3+} in disordered $\text{NaLu}(\text{WO}_4)_2$. *J. Appl. Phys.* **2008**, *103*, 083110:1–083110:8.
6. Wei, Y.W.; Chen, Y.J.; Lin, Y.F.; Gong, X.H.; Luo, Z.D.; Huang, Y.D. Spectral properties of Tm^{3+} -doped $\text{LiLa}(\text{MoO}_4)_2$ crystal. *J. Alloy. Compd.* **2009**, *484*, 529–534.
7. Zhu, H.M.; Chen, Y.J.; Lin, Y.F.; Gong, X.H.; Luo, Z.D.; Huang, Y.D. Spectral properties and efficient laser operation near 2.0 μm of $\text{Tm}^{3+}:\text{BaGd}_2(\text{MoO}_4)_4$ crystal. *J. Opt. Soc. Am. B* **2008**, *25*, 801–809.

8. Tang, J.F.; Chen, Y.J.; Lin, Y.F.; Gong, X.H.; Huang, J.H.; Luo, Z.D.; Huang, Y.D. Polarized spectral properties and laser demonstration of Tm³⁺-doped LiGd(MoO₄)₂. *J. Opt. Soc. Am. B* **2010**, *27*, 1769–1777.
9. Lagatsky, A.A.; Calvez, S.; Gupta, J.A.; Kisel, V.E.; Kuleshov, N.V.; Brown, C.T.A.; Dawson, M.D.; Sibbett, W. Broadly tunable femtosecond mode-locking in a Tm:KYW laser near 2 μm. *Opt. Express* **2011**, *19*, 9995–10000.
10. Koopmann, P.; Peters, R.; Petermann, K.; Huber, G. Crystal growth, spectroscopy, and highly efficient laser operation of thulium-doped Lu₂O₃ around 2 μm. *Appl. Phys. B* **2011**, *102*, 19–24.
11. Batay, L.E.; Demidovich, A.A.; Kuzmin, A.N.; Ryabtsev, G.I.; Strek, W.; Titov, A.N. Passive Q-switching of laser diode pumped LBGM:Nd Laser. *Spectrochim. Acta A* **1998**, *54*, 2117–2120.
12. García-Cortés, A.; Cascales, C. Crystal growth and optical and spectroscopic characterization of the ytterbium-doped laser molybdate Yb-Li₃Gd₃Ba₂(MoO₄)₈. *Chem. Mater.* **2008**, *20*, 3884–3891.
13. García-Cortés, A.; Zaldo, C.; Cascales, C.; Mateos, X.; Petrov, V. Laser operation of Yb³⁺ in disordered Li_{0.75}Gd_{0.75}Ba_{0.5}(MoO₄)₂ crystal with small quantum defect. *Opt. Express* **2007**, *15*, 18162:1–18162:7.
14. Song, M.J.; Zhao, W.; Wang, G.F.; Zhao, M.L.; Wang, L.T. Growth, thermal and polarized spectral properties of Nd³⁺-doped Li₃Ba₂Gd₃(MoO₄)₈ crystal. *J. Alloy. Compd.* **2011**, *509*, 2164–2169.
15. Song, M.J.; Wang, L.T.; Zhao, W.; Wang, G.F.; Zhao, M.L.; Meng, Q.G. Growth and spectroscopic properties of Er³⁺-doped Li₃Ba₂Y₃(MoO₄)₈ crystal. *Mater. Sci. Eng. B* **2011**, *176*, 810–815.
16. Rico, M.; Han, X.M.; Cascales, C.; Esteban-Betegón, F.; Zaldo, C. Efficient mid-infrared laser operation of Li₃Lu_{3-x}Tm_xBa₂(MoO₄)₈ disordered crystal. *Opt. Express* **2011**, *19*, 7640–7645.
17. Han, X.M.; Calderón-Villajos, R.; Esteban-Betegón, F.; Cascales, C.; Zaldo, C. Crystal growth and physical characterization of monoclinic Li₃Lu₃Ba₂(MoO₄)₈: A spectrally broadened disordered crystal for ultrafast mode-locked lasers. *Cryst. Growth Des.* **2012**, *12*, 3878–3887.
18. Judd, B.R. Optical absorption intensities of rare-earth ions. *Phys. Rev.* **1962**, *127*, 750–761.
19. Ofelt, G.S. Intensities of crystal spectra of rare-earth ions. *J. Chem. Phys.* **1962**, *37*, 511–520.
20. Braud, A.; Girard, S.; Doualan, J.L.; Moncorgé, R. Spectroscopy and fluorescence dynamics of (Tm³⁺, Tb³⁺) and (Tm³⁺, Eu³⁺) doped LiYF₄ single crystals for 1.5-μm laser operation. *IEEE J. Quantum Electron.* **1998**, *34*, 2246–2255.
21. McCumber, D.E. Einstein relations connecting broadband emission and absorption spectra. *Phys. Rev.* **1964**, *136*, A954–A957.
22. Pujol, M.C.; Bursukova, M.A.; Güell, F.; Mateos, X.; Solé, R.; Gavalda, J.; Aguiló, M.; Massons, J.; Díaz, F.; Klopp, K.; *et al.* Growth, optical characterization, and laser operation of a stoichiometric crystal KYb(WO₄)₂. *Phys. Rev. B* **2002**, *65*, 165121:1–165121:11.